Van der Pol Realization of Torus Knot Oscillators

RASSA RASSAI AND ROBERT W. NEWCOMB, FELLOW, IEEE

Abstract — **Van der Pol type nonlinear oscillators are used for the design of a torus knot oscillator. This involves replacing the structurally unstable linear oscillators of previous theories by nonlinear Van der Pol ones which can be designed using an op amp realized piecewise-linear negative resistor. The resulting five design cases are then conveniently treated using piecewise-linear theory to yield limit cycles from which the torus knots are formed. The resulting equations are used to obtain computer generated torus knot trajectories.**

I. Introduction

IN THEIR everyday lives, humans frequently tie knots, for example, in wrapping packages, putting on shoes, weaving, tieing boats to a dock, etc. As robots take over some of these jobs especially in conditions hazardous to humans, clearly there will be times when it will be desired to have robots forming knots. Consequently, it seems of interest to have electronic signals available which describe knots so that these may be applied as the need arises, perhaps in the coordinated motion of knot-tieing robot arms. Among the knots the most frequently met are the torus knots, so here we discuss a technique to practically obtain electronic signals that describe a torus knot.

Already it is known that a torus knot oscillator can be realized electronically by the use of two linear oscillators [1]. However, the system obtained is not too practical since it is not structurally stable, that is, with the slightest perturbation in the initial conditions there is a corresponding perturbation in the response. Since Van der Pol oscillators are known to be structurally stable [2], here, for the design of a torus knot oscillator, we use two nonlinear oscillators of Van der Pol type. Of importance is the characteristic of Van der Pol type nonlinear oscillators of having unique stable periodic solutions. We use this characteristic to design a torus knot oscillator and show that for any positive value of the Van der Pol parameter μ, we can obtain a torus knot oscillator. The resulting torus knot oscillator, obtained by employing two nonlinear oscillators of Van der Pol type, is structurally stable.

In Section II of this paper we give a brief review of the theory of linear torus knot oscillators. In Section III, we replace the linear oscillators with nonlinear oscillators of Van der Pol type and by the use of computer aided design methods we find the unique periodic solution of the Van der Pol type oscillator. Section IV contains considerations for the electronic circuit design of the resulting nonlinear torus knot oscillator.

Manuscript received August 7, 1986; revised May 27, 1987. This work was supported by the National Science Foundation under Grant ECS and MIP 85-06924. This paper was recommended by Associate Editor R. M. Sirsi.

The authors are with Microsystems Laboratory, Electrical Engineering Department, University of Maryland, College Park, MD 20742.

IEEE Log Number 8718329.

II. Review of Linear Torus Knot Oscillators

A torus knot can be thought of as a closed trajectory on a torus [3]. As such it can be created by coupling closed curves that traverse two circles, the coupling being the direct product reduced from four-dimensional space down into three dimensions. And, since a torus is anything that is topologically equivalent to the direct product of two circles, we can actually realize a torus knot by coupling trajectories on ellipses or square-like closed curves. With these ideas on hand we see that a torus knot oscillator can be realized electronically by the use of two linear oscillators of the form given by (1) [1]:

$$dx/dt = y \tag{1a}$$

$$dy/dt = -(\omega_1)^2 x \tag{1b}$$

$$dz/dt = w \tag{1c}$$

$$dw/dt = -(\omega_2)^2 z. \tag{1d}$$

In $x-y-z-w$ space, (1) generates the direct product of two circles, defined by (2) and (3):

$$(\omega_1 x)^2 + y^2 = (R_1)^2 \tag{2}$$

$$(\omega_2 z)^2 + w^2 = (R_2)^2. \tag{3}$$

Here the radii R_1 and R_2 are fixed by the initial conditions. The $x-y$ plane circle is traversed at a radian frequency ω_1 and the $z-w$ plane one is traversed at a radian frequency ω_2. Equations (1)–(3) describe a torus in real four-dimensional Euclidean space R^4, [4, p. 161], and, therefore, they describe a (ω_1, ω_2)-torus knot. To define the trajectories on a torus in the real three-dimensional Euclidean space R^3, we follow Parris [5] and introduce the following reduction from four to three dimensions:

Let

$$D = w + \Delta, \qquad \Delta = \text{constant} \tag{4}$$

0098-4094/88/0200-0215$01.00 ©1988 IEEE

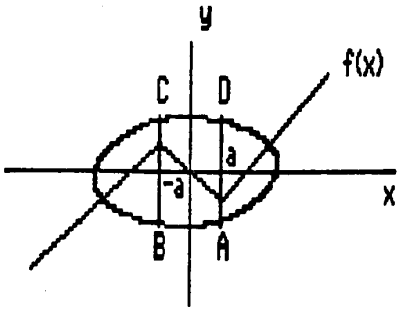

Fig. 1. Van der Pol type nonlinearity $f(X)$.

and

$$x = x/D \tag{5a}$$

$$y = y/D \tag{5b}$$

$$z = z/D \tag{5c}$$

$$X = \omega_1 x \tag{6a}$$

$$Y = y \tag{6b}$$

$$Z = (R_1\omega_2 z)/\left[\Delta^2 - R_2^2\right]^{1/2}. \tag{6c}$$

These give the following standard three-dimensional torus equation in terms of X, Y, and Z.

$$Z^2 + \left[R - \left[X^2 + Y^2\right]^{1/2}\right]^2 = r^2 \tag{7}$$

where

$$R = \Delta R_1/\left[\Delta^2 - R_2^2\right] \tag{8a}$$

$$r = R_1 R_2/\left[\Delta^2 - R_2^2\right]. \tag{8b}$$

Equation (7) is the equation of a torus in $X-Y-Z$ space with a meridian circle of radius r revolved around an axial circle of radius R with the axis of revolution being the Z axis. Therefore, (1) in conjunction with (4)–(6) comprise a set of semi-state equations for trajectories on a torus in the three-dimensional $X-Y-Z$ space. These trajectories form (ω_1, ω_2)-torus knots.

III. Van der Pol Type Oscillators

A. Defining Equations

Here we replace the two linear oscillators in the set of equations (1) by two Van der Pol type oscillators, where a Van der Pol type oscillator is defined via the following equations (9). In (9) μ is the Van der Pol parameter and $f(X)$ is the Van der Pol type nonlinearity which, because of its ease of realizability, here will be taken to be of the piecewise-linear form given by (10) and shown in Fig. 1; T is normalized time.

$$dX/dT = Y - \mu f(X) \tag{9a}$$

$$dY/dT = -X. \tag{9b}$$

One can look upon (9a), (9b) as being (1a), (1b) with $x = X$, $y = Y$, $t = T/w_1$ and the following nonlinearity

TABLE I
Variable and Parameter Choices for the Three Regions

Region	g	h	M
I (right)	X	Y+μK'	K
II (middle)	X	Y	-m
III (left)	X	Y-μK'	K

introduced:

$$f(X) = \begin{cases} KX - K', & X > a \quad (10a) \\ -mX, & -a < X < a \quad (10b) \\ KX + K', & -a < X. \quad (10c) \end{cases}$$

In these equations a, K, K', μ, m are positive constants.

With this type of nonlinearity a Van der Pol type oscillator has a unique periodic solution (a limit cycle in the $X-Y$ plane) and we use this characteristic of Van der Pol type oscillators to design a torus knot oscillator. For this we merely replace the two linear oscillators in (1) by two nonlinear oscillators of type (9)–(10), with different renormalizations of time (to yield the two different periods for traversal of the torus circles), and show that for any positive Van der Pol parameter, μ, we have knotted trajectories. Preliminary to this design we now proceed to discuss a computer-aided method for finding the periodic solution and the period of oscillation for a Van der Pol type oscillator with the piecewise nonlinearity of (10).

B. Periodic Solutions

With reference to the set of equations (9) and (10), there are three regions of the $X-Y$ plane corresponding to the three branches of $f(X)$, as shown in Fig. 1. Further we observe that there are three possible types of solutions in each region depending upon the slope of $f(X)$ in the region. Thus, in solving (9) we need to consider nine separate cases. However, in essence three cases suffice by making simple transformations from the $X-Y$ plane to a $g-h$ plane. Table I shows these transformations.

Therefore, we introduce the general set of differential equations (11), which, with reference to Table I, define the appropriate differential equations for each region of $f(X)$, as shown in Fig. 1.

$$dg/dT = h - \mu M g \tag{11a}$$

$$dh/dT = -g. \tag{11b}$$

Here, we should mention that in defining the actual solutions X and Y we use subscripts I, IIL, IIU, and III which mean solutions in region I, lower part of region II, upper part of region II and region III. The general solution to the set of differential equations (11) are of the following form

$$\begin{bmatrix} g(T) \\ h(T) \end{bmatrix} = e^{AT} \begin{bmatrix} g_0 \\ h_0 \end{bmatrix} \tag{12}$$

where

$$A = \begin{bmatrix} -\mu M & 1 \\ -1 & 0 \end{bmatrix} \tag{13}$$

and h_0 and g_0 are the initial conditions which will be defined later for each region of Fig. 1. The characteristic equation is given by (14):

$$s^2 + \mu M s + 1 = 0 \tag{14}$$

and the natural frequencies are given by the following equations:

$$s_1 = \left\{(-\mu M) + \left[(\mu M)^2 - 4\right]^{1/2}\right\}/2 \tag{15a}$$

$$s_2 = \left\{(-\mu M) - \left[(\mu M)^2 - 4\right]^{1/2}\right\}/2 \tag{15b}$$

for which we see from (14) that

$$s_1 + s_2 = -\mu M, \tag{15c}$$

$$s_1 \cdot s_2 = 1 \tag{15d}$$

To simplify the following development of solutions suitable to computer calculations we set

$$F = -\mu M/2, \tag{16a}$$

$$B = \left[(\mu M)^2 - 4\right]^{1/2}/2 \tag{16b}$$

$$= jC \tag{16c}$$

There are three cases to consider depending upon μM.

Case 1: $(\mu M)^2 > 4$

From (15), we have

$$s_1 = F + B \tag{17a}$$

$$s_2 = F - B \tag{17b}$$

and the general solutions to the set of differential equations (11) are found from (12), on using (15c), (15d), to be of the following form:

$$g(T) = \left\{e^{(F+B)T}\left[h_0 + g_0(F+B)\right] - e^{(F-B)T}\left[g_0(F-B) + h_0\right]\right\}/(2B) \tag{18a}$$

$$h(T) = \left\{-e^{(F+B)T}\left[g_0 + h_0(F-B)\right] + e^{(F-B)T}\left[g_0 + h_0(F+B)\right]\right\}/(2B). \tag{18b}$$

Case 2: $(\mu M)^2 = 4$

Then from (15) we have

$$s_1 = s_2 = F \tag{19}$$

where F is $+1$ or -1. The general solutions are of the following form.

$$g(T) = (Fg_0 + h_0)Te^{FT} + g_0 e^{FT} \tag{20a}$$

$$h(T) = -(g_0 + Fh_0)Te^{FT} + h_0 e^{FT} \tag{20b}$$

Case 3: $(\mu M)^2 < 4$

From (15) we have

$$s_1 = F + jC \tag{21a}$$

$$s_2 = F - jC. \tag{21b}$$

Here the general solutions to the set of equations (11) are again given by (18) which when expressed in real form are (22):

$$g(T) = h_0 e^{FT}\left[\sin(CT)(C + F * \tan\phi) + \cos(CT)(C * \tan\phi - F)\right] \tag{22a}$$

$$h(T) = h_0 e^{FT}\left[\cos(CT) - \sin(CT) * \tan\phi\right] \tag{22b}$$

where

$$\tan(\phi) = (g_0 + F * h_0)/(C * h_0). \tag{22c}$$

With these general solutions on hand we now consider Fig. 1 in order to find the periodic solution of the set of equations (9). We start at a point A, this being on a trajectory which we would like to be the limit cycle; for convenience we take A corresponding to the boundary of the right and middle region. Thus X_A, the X coordinate of A is known and to numerically determine the Y coordinate of the limit cycle we assume a value Y_A for it, and iterate upon Y_A. Therefore, we have the following:

$$X_A = X_{\text{IIL}}(0) = a \tag{23a}$$

$$Y_A = Y_{\text{IIL}}(0). \tag{23b}$$

To begin, we move clockwise on the limit cycle; while $-a < X < a$, $f(X)$ is given by (10b), and, therefore, we replace $f(X)$ in (9) by (10b); with reference to Table I we are in region II. Therefore, from Table I we make the proper substitutions to get the set of equations (11). Depending on the value of $(\mu M)^2$, we have three possible cases with the three different sets of solutions given by equations (18), (20), and (22). The initial values h_0 and g_0 are defined by (24):

$$g_0 = X_A = X_{\text{IIL}}(0) = a \tag{24a}$$

$$h_0 = Y_A = Y_{\text{IIL}}(0). \tag{24b}$$

Now, we continue moving on the chosen trajectory until at time $T = t_1$ we reach point B of Fig. 1. The X coordinate of B is equal $-a$ and we call the Y coordinate of B, Y_B, which is equal to $Y_{\text{IIL}}(t_1)$. These values will, therefore, be the initial conditions for the left region. For all $X < -a$, $f(X)$ is given by equation (10c). With reference to Table I, we make the proper substitutions for g and h in terms of X and Y to get the next set of differential equations (11). Here, again we have three different possibilities depending on the values of $(\mu M)^2$ and three subsequent sets of solutions given by equations (18), (20), and (22). g_0 and h_0 for region III are given by (25):

$$g_0 = X_B = X_{\text{IIL}}(t_1) = X_{\text{III}}(0) = -a \tag{25a}$$

$$h_0 = Y_B - \mu K' = Y_{\text{IIL}}(t_1) - \mu K' = Y_{\text{III}}(0) - \mu K'. \tag{25b}$$

The solution continues on the chosen trajectory until it reaches point C at some time $T = t_2$ for which $X_C = -a$ and $Y_C = Y_{\text{III}}(t_2)$. We then transfer to the middle region where again $-a < X < a$ and we have $f(X)$ given by (10b). The resulting differential equations are again transformed to (11) with the proper substitutions from Table I. Here, however, the initial conditions are the coordinates of

point C defined by

$$g_0 = X_C = X_{\text{III}}(t_2) = -a = X_{\text{IIU}}(0) \tag{26a}$$

$$h_0 = Y_C = Y_{\text{III}}(t_2) = Y_{\text{IIU}}(0). \tag{26b}$$

Moving further on the trajectory, we reach point D at $T = t_3$. The coordinates of point D become the initial conditions for the right region. We have

$$X_D = X_{\text{IIU}}(t_3) = a \tag{27a}$$

$$Y_D = Y_{\text{IIU}}(t_3). \tag{27b}$$

From Table I, and (10a), we make the proper substitutions for $f(X)$, g and h in the differential equations (11) and depending on the values of $(\mu M)^2$, we have our solution given by either equation (18) or (20) or (22). g_0 and h_0 for region I are given in the following form.

$$g_0 = X_{\text{IIU}}(t_3) = X_D = a = X_I(0) \tag{28a}$$

$$h_0 = Y_{\text{IIU}}(t_3) + \mu K' = Y_D + \mu K' = Y_I(0) + \mu K'. \tag{28b}$$

At $T = t_4$, we again reach $X = a$, hopefully at point A, where we originated our move. If $Y(t_4) \neq Y_A$ then we repeat the process by perturbing Y_A, increasing it if $Y(t_4) < Y_A$ or decreasing it if $Y(t_4) > Y_A$. This process of iteration is continued until $Y(t_4) = Y_A$ to within an acceptable error. According to [2], there exists a limit cycle, that is, a periodic solution, for all positive values of a, m, μ, K and K'. Therefore, with enough iterations and within a prescribed error we are able to find this periodic solution for any value of positive constants a, μ, m, K, and K'.

If our assumption of being on the limit cycle is true, we have the following:

$$X_I(t_4) = X_A = X_{\text{IIL}}(0) = a \tag{29a}$$

$$Y_I(t_4) = Y_A = Y_{\text{IIL}}. \tag{29b}$$

Because of the assumed symmetry of $f(X)$, we have

$$Y_A = -Y_C. \tag{30}$$

The limit cycle looks very much like a circle for μ small and for larger values of μ looks like a rectangle, as with the standard Van der Pol oscillator [6].

Now, we proceed to give the theory for the design of a torus knot oscillator, using the Van der Pol type oscillator whose limit cycles we are able to determine by the above equations.

IV. Design of a Torus Knot Oscillator

For the design of a torus knot oscillator we begin with two identical Van der Pol type oscillators in two different time frames of the following form:

$$dX/dT = Y - \mu f(X) \tag{31a}$$

$$dY/dT = -X \tag{31b}$$

$$dZ/dT' = W - \mu f(Z) \tag{32a}$$

$$dW/dT' = -Z. \tag{32b}$$

In (31) and (32), $f(\cdot)$ is defined by the set of equations (10) and is shown in Fig. 1. The period of oscillation of the oscillators defined by (31) and (32) is the same; call it T_P. Since we want to design a (ω_1, ω_1)-torus knot oscillator, we time scale each oscillator separately, that is, we write the following transformations:

$$T = \omega_1 t \tag{33a}$$

$$X = x \tag{33b}$$

$$Y = y \tag{33c}$$

$$T' = \omega_2 t \tag{34a}$$

$$Z = z \tag{34b}$$

$$W = w \tag{34c}$$

where now t is the true time.

Using (33) and (34), and making the proper substitutions in equations (31) and (32) we have the following four-dimensional description of our knot in true time t.

$$dx/dt = \omega_1(y - \mu f(x)) \tag{35a}$$

$$dy/dt = -\omega_1 x \tag{35b}$$

$$dz/dt = \omega_2(w - \mu f(z)) \tag{36a}$$

$$dw/dt = -\omega_2 z. \tag{36b}$$

We call the true period of oscillation of the oscillator defined by (35), T_1, and call its frequency of oscillation Ω_1. Similarly, using subscripts 2 for the other oscillator, on using (33) and (34), we have

$$T_1 = T_P/\omega_1 \tag{37a}$$

$$\Omega_1 = 2\pi\omega_1/(T_P) \tag{37b}$$

$$T_2 = T_P/\omega_2 \tag{38a}$$

$$\Omega_2 = 2\pi\omega_2/(T_P). \tag{38b}$$

Following [1], the set of equations (35)–(36) describe a torus in the real four dimensional Euclidean space, R^4. The $x-y$ plane limit cycle is traversed at the radian frequency Ω_1 and the $z-w$ plane limit cycle is traversed at the radian frequency Ω_2. We then impose the constraints of (4) and (5) which reduces the torus from four to three dimensions. It should be noticed that since the Van der Pol type oscillators' limit cycles are not quite circles the resulting torus is not quite a circle revolved around another circle but is a closed path revolved around another similar closed path, and, hence, is equivalent to the torus. For very small values of μ we essentially do have a meridian circle revolved around an axial circle. However, for large values of μ we have a meridian rectangle revolved around an axial rectangle. In any event equations (35) and (36), in connection with (4) and (5), describe a (Ω_1, Ω_2)-torus knot, which is equivalent to a (ω_1, ω_2)-torus knot. The latter equivalence results from the fact that $\Omega_1/\Omega_2 = T_2/T_1 = (\omega_1/T_P)/(\omega_2/T_P) = \omega_1/\omega_2$ where we take ω_1 and ω_2 to be prime integers. It is to be noted that T_P cancels out, and, hence, knowledge of its value is not needed to insure that a torus knot results.

Using (11)–(38) we have designed a computer program which draws a (ω_1, ω_2)-torus knot. In this program we find the limit cycles for a given value of μ graphically. One limit cycle is in the $x-y$ plane and the second limit cycle

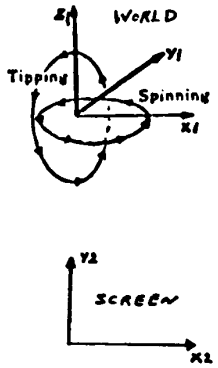

Fig. 2. Spinning and tipping.

is in the $z-w$ plane. Starting at the time $t=0$, and then incrementing t, we used the set of equations (4)–(6) to plot a point on the torus in the three dimensional space. We call the coordinates of this point world coordinates ($X1, Y1, Z1$) in the three-dimensional world space in which the torus is placed. From (4) we notice that Δ is a constant. However, Δ need not be a constant and can be a function of x, y, z, w.

In the program we set $\Delta = (x^2 + y^2 + z^2 + w^2)^{1/2}$ and we have used viewing transformations that take us from our three-dimensional world coordinates to the two-dimensional coordinates of the screen, here called ($X2, Y2$). The viewing transformations have been broken up into three sub-transformations: first one or two 3-D to 3-D rotations, then a three- to two-dimensional parallel projection, and finally a standard 2-D viewing transformation onto the screen. Every 3-D rotation is characterized by a world axis of rotation and a world plane of rotation as shown in fig. 2. There are rotations whose plane of rotation is one of the principal planes formed by the world coordinate axes. We will use two of these: spinning and tipping. For spinning, the plane of rotation is the $X1-Y1$ plane and for tipping, the plane of rotation is the $Y1-Z1$ plane [7]. A spin of zero and a tip of 90 degrees will show the top view of the knot, that is, the projection of the knot on the $X1-Y1$ plane, which becomes the $X2-Y2$ screen plane. Spin = 90, tip = 0, will show the side view of the knot, that is, the projection of the knot on the $Y1-Z1$ plane, which in this case is the $X2-Y2$ screen plane. Spin = 0, tip = 0 will show the front view of the knot, that is, the projection of the knot on the $X1-Z1$ plane, which will become the $X2-Y2$ screen plane [7]. The top views of (3,4)-, (4,3)-, and (11,10)-torus knots are shown in Fig. 3(a), 3(b), and 3(c). From Fig. 3 we notice that the top view projections of all these knots are in regular positions, and the (3,4)- and (4,3)-torus knots are topologically equivalent, [5] and [8]. In the case of the (11,10)-torus knot shown in Fig. 3(c) the actual shape of a torus on which the knot is tied is quite clear.

Fig. 4(a) and 4(b) show the front and side views of the projected images of a (4,3)-torus knot on the $X1-Z1$ and the $Y1-Z1$ world coordinate planes. Even though this knot is not shown in its regular position in these figures it

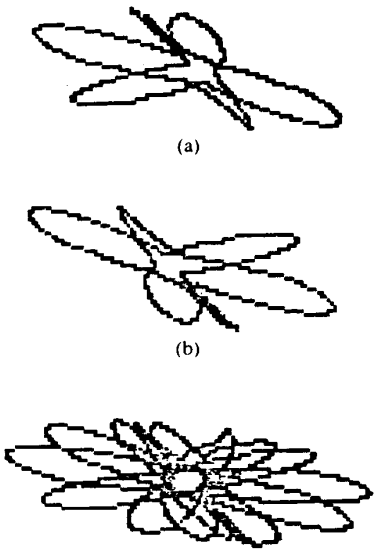

(a) (b) (c)

Fig. 3. Typical torus knot trajectories, $p=3$. (a) (3,4)-top view. (b) (4,3)-top view. (c) (11,10)-top view.

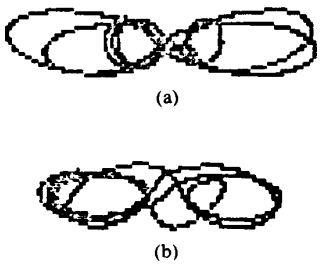

(a) (b)

Fig. 4. (a) (4,3)-front view. (b) (4,3)-side view.

is evident that the trajectories travel four times along the meridian circle and three times along the axial circle. From these figures it is also clear that all the trajectories close upon themselves.

With reference to (35) and (36), we observe that for the electronic circuit realization we need to give the circuit design for $f(X)$ and $f(Z)$. For these functions we have followed the theory given in [9] based upon the op amp negative resistor of Endo [10, p. 15]. The detailed electronic circuit design of $f(X)$ and $f(Z)$ and a (ω_1, ω_2)-torus knot are given in [8].

V. Discussion

Here, we have used two nonlinear oscillators of Van der Pol type to design a torus knot oscillator. Van der Pol type nonlinear oscillators are structurally stable, and, therefore, the system of torus knot oscillators, as a whole, is a more practical system than one constructed from linear oscillators. It should be noted that since we do not know how to determine the period of a Van der Pol oscillator analytically we have used identical oscillators as a base since these have identical periods. Then by a time scale change

on each oscillator we have been able to get desired ratios of periods, these being what are needed for the torus knot oscillators. Thus even though we do not know the exact period it is immaterial since only the ratios matter and in the ratios the Van der Pol period cancels out when we use identical oscillators. In the electronic circuit design of a (ω_1, ω_2)-torus knot [8], the ratio of ω_1 to ω_2 for the realized knot, is obtained as a ratio of resistors. This ratio must be rational for the trajectory to be a knot, since if the ratio is irrational the trajectories never close upon themselves. On the computer of course we can obtain precisely a rational number but in experimental practice it is a philosophical question, with various paradoxical responses, as to whether such can ever be obtained. However, to the resolution of our oscilloscope trace we obtain closed trajectories from the actual electronic circuits realizing the knots, and this should be satisfactory for practical applications of the knot theory developed here. Although this question of whether rational or irrational ratios are obtained is a philosophical question, it is a fascinating one of considerable practical interest since experimentally one may someday need to know whether an irrational number is (or even can be) precisely implemented; but any experimental technique probably lacks the resolution to determine as to whether a number is irrational or rational since the latter are dense in the former. Still, in theory some results, such as the closure of our trajectories into knots, depend upon having a rational rather than an irrational number implemented.

In the above we have assumed a symmetric nonlinearity $f(X)$. This is primarily for clarity of the presentation and is not necessary for the actual operation of the knot operators as long as there is a negative resistance region surrounded by two positive resistance regions.

References

[1] R. W. Newcomb, "Design of a torus knot oscillator," in *Proc. 27th Mid-West Symp. on Circuits and Systems*, Morgantown, WV, vol. 1, pp. 344–347, June 1984.

[2] N. Minorsky, *Nonlinear Oscillations*. Princeton, NJ: Van Nostrand, 1962.

[3] H. Seifert and W. Threlfall, *A Textbook of Topology*. New York: Academic, 1980.

[4] V. I. Arnold, *Ordinary Differential Equations*. Cambridge, MA: The MIT Press, 1973.

[5] R. Parris, "A three dimensional system with knotted trajectories," *Amer. Math. Mthly.*, vol. 84, no. 6, June–July 1977.

[6] B. Van der Pol, "The nonlinear theory of electric oscillations," in *Proc. Inst. Radio Eng.* vol. 22, no. 9, pp. 1051–1086, Sept. 1934.

[7] M. Waite and C. L. Morgan, *Graphics Primer for the IBM PC*. Berkeley, CA: McGraw-Hill, pp. 468–469, 1983.

[8] R. Rassai, "Theory and electronic circuit design of multi-torus knot oscillators," Ph.D. dissertation, Univ. of Maryland, December 1985.

[9] R. W. Newcomb, "Bent hysteresis and its realization," *IEEE Trans. Circuits Syst.*, vol. CAS-29, July 1982, pp. 478–482, July 1982.

[10] T. Endo and S. Mori, "Mode analysis of a ring of a large number of mutually coupled Van der Pol oscillators," *IEEE Trans. Circuits Syst.*, vol. CAS-25, pp. 7–18, Jan. 1978.

Rassa Rassai received the B.S.E.E. degree in 1973, the M.S.E.E. degree in 1975, and the Ph.D. degree in electrical engineering in 1985 from the University of Maryland, College Park.

She is currently a Research Associate at the University of Maryland in the Department of Electrical Engineering. Her research interests are knot theory and applications of semistate theory in the design, and the theoretical development of microelectronic circuits.

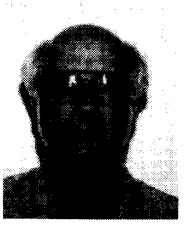

Robert W. Newcomb (S'52–M'56–F'72) was born in Glendale, CA, in 1933 received the B.S.E.E. degree from Purdue University, IN, in 1955, the M.S. degree from Stanford University, CA, in 1957, and the Ph.D. degree from the University of California, Berkeley, in 1960, all in electrical engineering.

He was a Research Intern at Stanford Research Institute, 1955–1957, and on the Faculties of Berkeley, 1957–1960, and Stanford, 1960–1970, before joining the University of Maryland. He has had Fulbright Fellowships to Australia and Malaysia and leaves to Belgium and Spain. He has chaired a number of international meetings in the systems theory area, is a founder of the Mathematical Theory of Networks and Systems International Symposium, and a founding member of the IEEE Council on Robotics and Automation. Recently in Spain he has set up a robotics laboratory while organizing the research faculty "Grupo de Trabajo en Sistemas PARCOR," directing its activities primarily in the robotics and biomedical signal processing areas within the computer faculty of the Universidad Politécnica de Madrid. His present research concentrates upon nonlinear semistate theory and its applications to various areas such as neural-type microelectronics, biomedical signal processing, and robotics.

Dr. Newcomb is a Registered Professional Engineer in California.